

Mapping Root Zone Soil Moisture Using Remotely Sensed Optical Imagery

Christopher A. Scott¹; Wim G. M. Bastiaanssen²; and Mobin-ud-Din Ahmad³

Abstract: Field-based soil moisture measurements are cumbersome. Remote sensing techniques based on active or passive microwave data have limitations. This paper presents and validates a new method based on land surface energy balances using remotely sensed optical data (including thermal infrared), which allows field and landscape-scale mapping of soil moisture depth-averaged through the root zone of existing vegetation. Root zone depth can be variable when crops are emerging. The pixel-wise “evaporative fraction” (ratio of latent heat flux to net available energy) is related to volumetric soil moisture through a standard regression curve that is independent of soil and vegetation type. Validation with measured root zone soil moisture in cropped soils in Mexico and Pakistan has a root mean square error of $0.05 \text{ cm}^3 \text{ cm}^{-3}$; the error is less than $0.07 \text{ cm}^3 \text{ cm}^{-3}$ in 90% of cases. Consequently, soil moisture data should be presented in class intervals of $0.05 \text{ cm}^3 \text{ cm}^{-3}$. The utility of this method is demonstrated at the field scale using multitemporal thematic mapper imagery for irrigated areas near Cortazar in Mexico, and for river basin-scale water resources distribution in Pakistan. The potential limitation is the presence of clouds and the time lag between consecutive images with field-scale resolution. With the falling price of optical satellite imagery, this technique should gain wider acceptance with river basin planners, watershed managers, and irrigation and drainage engineers.

DOI: 10.1061/(ASCE)0733-9437(2003)129:5(326)

CE Database subject headings: Soil water; Remote sensing; Irrigation; Watersheds; Water resources; Mapping; Imaging techniques.

Introduction

Soil moisture is a key hydrologic parameter linked to water availability, land surface evapotranspiration, runoff generation, groundwater recharge, and irrigation scheduling among other processes. Knowledge of the actual soil moisture conditions significantly helps in quantifying a range of hydrological processes and indicates where water is physically present in watersheds and river basins. The deviation between actual and desirable values of soil moisture is critical for the water resources management decision-making process. Wetlands should be wet to conserve native vegetation and habitats, agricultural soils should be sufficiently drained to prevent waterlogging and control salinity, while irrigation may be necessary to supplement soil moisture when root water uptake is below the limit that results in crop yield reductions.

Water conservation and management strategies require information on the use and flow paths of water. Soil moisture patterns can help in the delineation of hydromorphic zones (Molden et al.

2001), an emerging tool for integrated water management decision making in river basins. Although the need for integrated water resources management is recognized and is currently being promoted, it is highly questionable whether sufficient data exist or can effectively be collected at the watershed or river basin level to actually operationalize integrated management.

Data scarcity is more the rule than the exception for hydrological studies and modeling applications alike (Arnold et al. 1993; Refsgaard 1997). Upper catchments in river basins generally act as runoff-generating areas. Knowledge of the spatial patterns of soil moisture is of immense importance to understand how much water is stored and captured in uplands as a means to partition water retained upstream, runoff available to downstream users, and recharge of groundwater. Flood prediction, including information on the spatial extent of inundation, discharge, and timing of the flood peak, and duration of recession, is critically dependent on soil moisture data. Similarly, changes in soil moisture at the land-atmosphere boundary are of critical importance to the parametrization of weather prediction and climate models (Oki et al. 1999; Walker and Houser 2001).

Soil moisture is subject to rapid changes in time (t) and shows significant variability with depth (z) and space (x, y). A complete description of soil moisture behavior, therefore, requires frequent (t) and multiple three-dimensional (x, y, z) measurements. The most advanced in situ soil moisture methods describe only the temporal variability at one given location, i.e., when probes are permanently installed in the soil profile at a particular place. The spatial variability across large watershed areas cannot be assessed by in situ measurement techniques.

As a consequence of the gap between desirable and available soil moisture data, remote sensing applications for soil moisture retrieval have been evolving. The majority of the remote sensing soil moisture models are applicable for the very shallow topsoil only, i.e., the upper few centimeters of the soil profile. Many

¹Principal Researcher, International Water Management Institute (IWMI), c/o ICRISAT, Patancheru, AP 502 324, India. E-mail: c.scott@cgiar.org

²Senior Research Fellow, IWMI, P.O. Box 2075, Colombo, Sri Lanka. E-mail: w.bastiaanssen@cgiar.org

³Water Resources Engineer (GIS/RS), IWMI, 12 km Multan Road, Lahore 53700, Pakistan. E-mail: a.mobin@cgiar.org

Note. Discussion open until March 1, 2004. Separate discussions must be submitted for individual papers. To extend the closing date by one month, a written request must be filed with the ASCE Managing Editor. The manuscript for this paper was submitted for review and possible publication on April 2, 2002; approved on August 16, 2002. This paper is part of the *Journal of Irrigation and Drainage Engineering*, Vol. 129, No. 5, October 1, 2003. ©ASCE, ISSN 0733-9437/2003/5-326-335/\$18.00.

Table 1. Overview of Remote Sensing Techniques to Estimate Soil Moisture Based on Different Parts of Electromagnetic Spectrum

Spectrum	Advantage	Disadvantage
Passive microwave	<ul style="list-style-type: none"> All weather conditions technique Good physical basis 	<ul style="list-style-type: none"> Soil moisture only retrievable from the top layer and for light vegetation Large pixel size from satellites Aircraft acquisitions are expensive
Active microwave (SAR)	<ul style="list-style-type: none"> All weather conditions technique Good physical basis 	<ul style="list-style-type: none"> Moisture estimates affected by surface roughness Aircraft based measurements have a penetration depth limited to a few decimeters Satellite based measurements are expensive
Visible	<ul style="list-style-type: none"> Simple to operate Applicable at a range of spatial and temporal scales 	<ul style="list-style-type: none"> Cloud free conditions required Strong empirical character
Thermal infrared	<ul style="list-style-type: none"> Provides an integrated soil moisture value for the root zone Good physical basis Applicable at a range of spatial and temporal scales Cost effective technique 	<ul style="list-style-type: none"> Cloud free conditions required Depth of the root zone is variable across an image

hydrological, environmental and agricultural applications, as mentioned however, require information on the root zone soil moisture content, which coincides with approximately the first meter of soil depth at a resolution of one hectare or finer and over wide spatial scales. This requires the pixel dimension to be less than 100 m, and limits the selection of satellite platforms to those that collect data at high spatial resolution. Conventionally, high-resolution soil moisture studies are based on synthetic aperture radar (SAR) measurements (e.g., Moran et al. 2002). At present (December 2002), there are only two operational SAR-based satellite producing images with the C band (RadarSat and EnviSat); these are of limited utility for soil moisture applications (see below) and are relatively expensive. The situation will likely change in the future when more SAR systems are launched.

This paper attempts to semioperationally assess the root zone soil moisture content using optical imagery. The method developed and validated here for irrigated conditions in central Mexico and Pakistan could be applied to other land and soil moisture regimes. The advantage of using optical imagery as opposed to

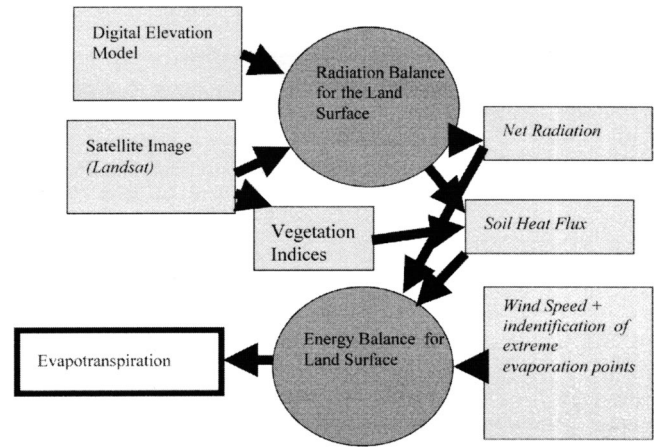


Fig. 1. Schematic summary of surface energy balance algorithm for land computational process for determining evapotranspiration (after Morse et al. 2000)

radar is that large archives of high-resolution data exist and continue to be collected operationally, e.g., landsat thematic mapper (TM) imagery since 1982, and advanced space-borne thermal emission and reflection radiometer (ASTER) since 2000. The innovative elements of this method are: (1) the derivation of soil moisture content, depth-averaged throughout the root zone of standing vegetation with high spatial resolution (30 m × 30 m) and broad coverage (multiple km²); (2) multitemporal coverage over vegetative or crop growth cycles; (3) the use of routinely available satellite imagery; and (4) the low costs of data acquisition and processing (e.g., ASTER imagery is currently distributed for U.S.\$55 per scene by the U.S. Geological Survey Center).

Existing Remote Sensing Soil Moisture Models

The basis for microwave remote sensing of soil moisture is the strong dependence of the soil's dielectric properties on its moisture content. The contrast between the dielectric constant of water and that of dry soil is great; soil moisture is thus clearly manifested through the dielectric properties. Microwave techniques have the strong advantage of being able to penetrate clouds, which is extremely useful in humid regions and at higher latitudes with frequently cloud covered skies. Operational microwave technologies from remote platforms have wavelengths in the range of a few centimeters to a few decimeters (C, L, P bands are equivalent to 5.6, 21, and 68 cm or 5.3, 1.4, 0.438 GHz, respectively). Due to these limited wavelengths, microwave techniques can only provide estimates of the near-surface soil moisture content, i.e., the upper few centimeters of the soil profile (e.g., Engman and Chauhan 1995; Njoku and Entekhabi 1996; Jackson 1997).

Soil moisture estimates can be obtained with airborne passive radiometers for soil depths between 0 and 10 cm (e.g., Schmugge 1999). Under denser vegetation, the effect of leaf water content becomes dominant and the technique is therefore more suitable for sparse vegetation cover. The shallow depth of 10 cm is insufficient to obtain root zone soil water storage, as many crops root up to 100 cm deep or more, and the soil moisture conditions over these depths behave essentially independently from the near-surface soil moisture. Another clear limitation of this technique is that special airborne missions must be organized, given that spaceborne microwave radiometers have a resolution varying be-

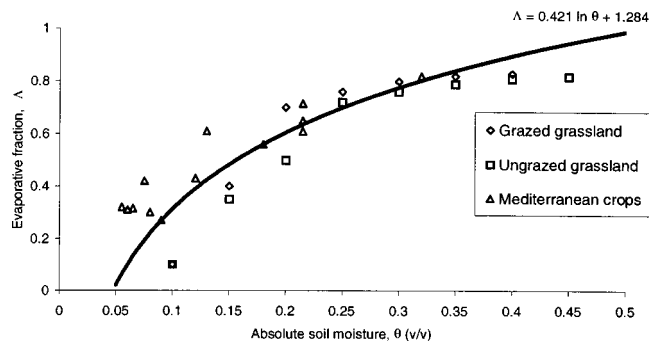


Fig. 2. Exponential relationship between volumetric soil moisture and evaporative fraction obtained from experimental data collected in Kansas first international satellite land surface climatology project field experiment and Spain ECHIVAL field experiment in densification-threatened areas

tween 50 and 150 km. The need to pay for special flights with passive radiometers to allow data acquisition at roughly 50 m resolution makes frequent moisture surveying on an operational basis infeasible and unaffordable.

Active radar transmits an electromagnetic pulse that is directionally scattered and reflected off rough surfaces. Multiple frequency and polarization observations are required to simultaneously retrieve small-scale roughness and dielectric properties. The 20–30 m spatial resolution of active microwave sensors in the form of radars aboard the European remote sensing (ERS) satellite, Japan Earth resources (JERS) satellite, RadarSat, and EnviSat is very good. The ERS and JERS satellites are, however, no longer operational. Promising results for bare soils are reported by for instance Su et al. (1997) and Mancini et al. (1999). The C-band wavelength of 5.6 cm used by these sensors is insufficient to penetrate the vegetation layer and the backscatter coefficient is significantly affected by surface roughness (Ulaby and Elachi 1990; Verhoest et al. 1998; Hoeben and Troch 2000). Generally, the application of C-band SAR images is only suitable for “light vegetation”. Van Oevelen (1998) demonstrated that by combining airborne active microwave radar measurements with 68 cm waves (P band), it is possible to estimate soil moisture integrated over a layer of 17 cm depth; however, this is still considered shallow. Moreover, this solution requires expensive aircraft operation because the P-band radar is not operationally

Table 2. Soil Characteristics, Moisture Ranges, and Vegetation Types Used to Determine Evaporative Fraction–Soil Moisture Relationship Shown in Fig. 2

Location	Soil type	Soil moisture range (cm ³ cm ⁻³)	Sensor depth (cm)	Vegetation/crop types
Kansas USA	Alluvial and loess	0.08–0.49	2.5	Ungrazed grassland
Kansas USA	Alluvial and loess	0.08–0.43	2.5	Grazed grassland
Castilla la Mancha, Spain	Loamy sand	0.06–0.32	10–50	Vineyard, barley, wheat, maize, alfalfa

available on satellite platforms. In general, the limitation of microwave methods is that they cannot be used to estimate soil moisture in the root zone under lush green vegetation, such as in agriculture or in wetlands and other environmentally sensitive zones.

Little attention has been paid to the use of surface temperature of vegetated surfaces for the determination of subsurface soil moisture. Mahfouf (1991) used a data assimilation technique to infer surface soil moisture from the surface energy balance and temperature observations. Li and Islam (1999) worked on a similar technique. Despite the fact that substantial effort has been made to describe crop water stress using surface temperature as the primary variable (e.g., Jackson et al. 1977; 1981; Moran et al. 1994), quantitative assessments of soil moisture using crop water stress parameters as intermediate variables are not common. The converse is, however, often applied in agro-hydrological studies where soil moisture is used to reduce potential evapotranspiration to actual evapotranspiration (e.g., Belmans et al. 1983; Wagenet and Hutson 1996; Allen 2000; Sarwar et al. 2000). On similar grounds, it can be argued that the difference in actual and potential evapotranspiration is caused by soil water stress. Further, the moisture that is transported to allow transpiration through the canopy originates throughout the vegetative root zone, typically one meter for most fully established irrigated crops. However, the actual root zone depth will depend on the stage of crop or vegetative development and could be less than 1 m. Mature forest systems may on the contrary root much deeper and can go up to a few meters. Thus, it is critical to emphasize that comparison of remotely sensed estimates of actual and potential evapotranspiration should be suitable to infer root zone soil moisture.

On the basis of the extensive availability of Landsat imagery with its associated thermal infrared measurements and favorable spatial resolution of 30 m (60–120 m in the thermal infrared band), a soil moisture module related to the surface energy balance will be further elaborated. The primary requirement is an adequate description of the surface energy balance prevailing under actual environmental conditions. This approach, based on the principle that the partitioning of surface heat fluxes is an indication of soil moisture conditions, is not new. Earlier achievements were reported by Davies and Allen (1973) for agricultural soils in Canada, de Bruin (1983) for pastures in The Netherlands, and Owe and van de Griend (1990) for semiarid watersheds in Botswana. All these studies are based on the Priestley–Taylor α parameter to describe actual evaporation under water stressed conditions as a function of soil moisture content. Kustas et al. (1999) worked on establishing a relationship between surface energy partitioning (they used the Bowen ratio for that) and near-surface soil moisture maps generated from passive microwave data collected during the Washita watershed in Oklahoma. Table 1 summarizes the practical feasibility of using various spectra to estimate soil moisture.

Soil Moisture Estimates from Surface Energy Balance Algorithm for Land

The surface energy balance algorithm for land (SEBAL) is an image-processing model comprised of 25 computational steps that calculates the actual and potential evapotranspiration (ET) and other energy exchanges at the earth’s surface using digital image data collected by Landsat or other remote-sensing satellites measuring visible, near-infrared and thermal infrared radiation. Surface energy balance algorithm for land algorithms compute a complete radiation and energy balance for the surface along with

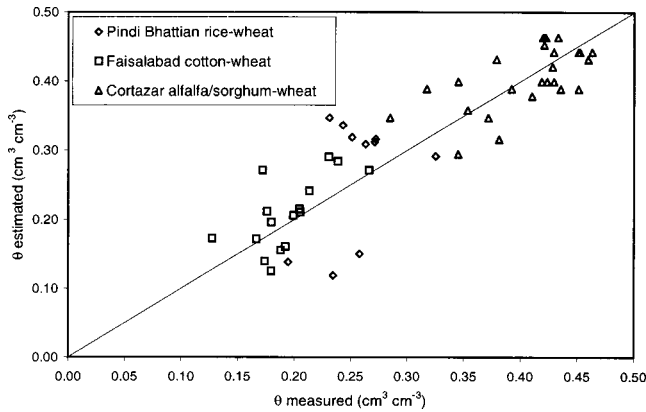


Fig. 3. Soil moisture (% v/v) measured in field by frequency domain radiometer (Pakistan) and capacitance probe (Mexico), and estimated from evaporative fraction using Eq. (3). In Pakistan evaporative fraction was measured in situ; in Mexico, evaporative fraction was derived from thematic mapper measurements ($n = 52$).

heat fluxes and resistances for momentum, heat and water vapor transport. Evapotranspiration is computed as a component of the energy balance on a pixel-by-pixel basis. Whereas ET_{act} is based on an energy balance residual term, ET_{pot} is based on a minimum surface resistance that is a function of leaf area index and reduction terms for ambient heat and water vapor stress. A general schematic of the SEBAL process is illustrated in Fig. 1. Detailed discussions are outside the scope of this publication; readers are referred to Bastiaanssen et al. (1998) and Bastiaanssen (2000) for a complete description of SEBAL.

The SEBAL procedure consists of a suite of equations that solve the complete energy balance

$$\lambda E = R_n - G - H \quad (1)$$

where λE = latent heat flux (the energy used to evaporate water); R_n = net radiation at the surface; G = soil heat flux; and H = sensible heat flux to the air. R_n is computed for each pixel using albedo and transmittances computed from short wave bands and using long wave emission computed from the thermal band. Soil heat flux is predicted using vegetation indices computed from spectral data and net radiation. Sensible heat is calculated from several factors: surface temperature and a single wind speed measurement at the ground, and estimated surface roughness and surface-to-air temperature differences predicted from thermal in-

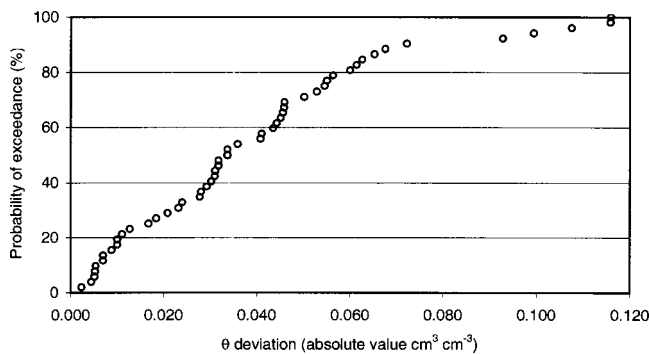


Fig. 4. Probability of exceeding certain deviation in soil moisture content (absolute value) based on validation data shown in Fig. 3 ($n = 52$)

Table 3. Thematic Mapper Image Acquisition Dates for Surface Energy Balance Algorithm for Land Soil Moisture Determinations in Mexico

Image	Date
TM 27/46	11 Feb 98
	25 Oct 98
	21 May 99
TM 28/45	01 Nov 98
	25 Mar 99
TM 28/46	22 Mar 98
	01 Nov 98
	25 Mar 99

frared radiances. All computations are made specific to each pixel in the image. Iterative predictions of sensible heat are improved using atmospheric stability corrections based on Monin–Obukhov similarity. Endpoints for H within a satellite image are bounded by known evaporative conditions at key reference points. These reference points include pixels having little or no evaporation. Specific solutions of Eq. (1) applies to recently burned areas (where $H \sim R_n - G$), desert areas having depleted soil water ($H \sim R_n - G$), fallow land that has not received rainfall ($H \sim R_n - G$), shallow water bodies ($H \sim 0$), and well irrigated fields (where $H \sim 0$ so that $\lambda E \sim R_n - G$). Evapotranspiration is finally calculated from λE by dividing by the latent heat of vaporization, λ . Applications of SEBAL are presented in Bastiaanssen et al. (2000); Morse et al. (2000); Allen et al. (2001); Bastiaanssen and Bandara (2001); and Bastiaanssen et al. (2002)

A first approximation of volumetric soil moisture is obtained using a statistical relationship between moisture and the evaporative fraction of latent heat/(net radiation minus soil heat flux). This relationship between energy partitioning and soil moisture for two large-scale field campaigns dedicated to soil moisture–evaporation–biomass interactions, first international satellite land surface climatology project field experiment (FIFE) and ECHIVAL field experiment in densification-threatened areas (EFEDA), is demonstrated in Fig. 2. The first international satellite land surface climatology project (ISCLCP) field experiment was held south of Manhattan on the Kansas prairie during 1987 and 1989 (Sellers et al. 1992) and aimed at developing models for land–surface–atmosphere interactions on regional and global scales. In a paper by Smith et al. (1992), in situ measured heat fluxes and soil moisture data from FIFE were presented; these data are included in Fig. 2. The data were collected from 22 surface flux stations at 20 sites during four intensive field campaigns conducted during 1987. The dominant land use was grassland and the soil types were essentially alluvial or eolic (see Table 2). Soil moisture was obtained by means of gravimetric measurements at 2.5 cm depth. The prairie contained a stratification of grazed and ungrazed sites where the root depth is considered to be very shallow.

A field campaign with similar goals, i.e., the ECHIVAL EFEDA project, was held in Castilla la Mancha (Central Spain) during the summer of 1991 (Bolle et al. 1993). This Mediterranean landscape contained rainfed (vineyard, barley, wheat) and irrigated crops (maize, alfalfa). Surface fluxes and soil moisture were measured in the rainfed agricultural landscape around Tomelloso ($n = 6$) and in pivot irrigated fields in Barrax ($n = 9$). Various international research centers and universities were part of the effort. Most surface fluxes were measured by eddy-

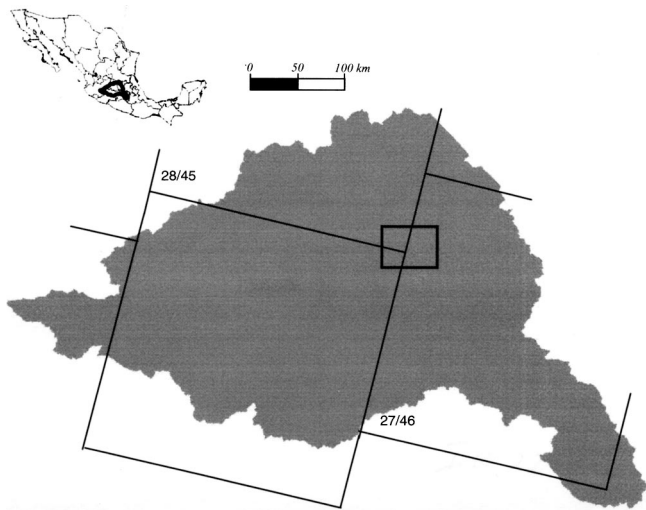


Fig. 5. Mexico study area showing thematic mapper image overlap

covariance systems, and some flux stations were equipped with a Bowen ratio or scintillometer system. Some research groups measured latent heat flux directly from the eddy covariance while other groups used the eddy covariance to measure sensible heat flux and compute latent heat flux as a residual term [similar to Eq. (1)] or obtained it from the Bowen ratio values. More information on the measurement techniques and the agreement with SEBAL-derived energy balance terms can be found in Pelgrum and Bastiaanssen (1996). Time domain reflectometers and neutron probes were installed at 18 individual plots in Tomelloso and 28 plots in Barrax (Droogers et al. 1993). Sensor readings were calibrated against gravimetric soil moisture measurements. The depth of the sensors varied with the type of crop; for deeper rooting crops, the sensors were installed at greater depth. However, the rocky subsoil did not permit the installation of moisture sensors (or the development of active roots) deeper than 50 cm. The relationship between evaporative fraction and soil moisture was originally derived by Bastiaanssen et al. (1997) using the validated evaporative fraction data from SEBAL and the in situ measured soil moisture data. The data from FIFE and EFEDA form the basis for Table 2 and Fig. 2. The source of soil moisture measurements in the creation and validation of the relationship originates from different depths, but this is in agreement with the depth-dependent root water extraction of standing vegetation. For bare soil conditions the moisture content was taken from a depth of 0–10 cm only.

The nonlinear behavior of the evaporative fraction $\Lambda(\theta)$ relationship demonstrates that little crop water stress exists if the soil is near saturation. A value of $\Lambda \geq 0.8$ is generally associated with favorable crop growing conditions without crop water stress. The evaporative fraction lies between 0.8 and 1.0 for absolute soil moisture ranging between 0.35 and 0.51 $\text{cm}^3 \text{cm}^{-3}$, respectively. Except for sandy soils, this moisture range typically reflects field capacity and conditions where plants have little or no soil moisture stress. Similar values were found by Monteny et al. (1997) in a catchment scale hydrology study in Niger. Hence, wet soil conditions in a range between field capacity and full saturation hardly affect Λ and ET; this agrees with the usual schematization that $\text{ET}_{\text{act}} - \text{ET}_{\text{pot}}$ if moisture is easily available (e.g., Allen et al. 1998).

Under normal weather conditions, the evaporative fraction cannot exceed one (only under advective conditions this may occur). According to the energy balance scaling between wet and

dry areas, an evaporative fraction of one ($H \sim 0$) applies to saturated surfaces such as water bodies, water logged land, wetlands, etc. This implies that the degree of moisture saturation reaches unity ($\theta/\theta_{\text{sat}} = 1.0$) and that the actual soil moisture θ should be equal to the soil porosity, i.e., $\theta = \theta_{\text{sat}}$. Extrapolation of the regression curve shown in Fig. 2 to $\Lambda = 1.0$, shows that $\theta = \theta_{\text{sat}} = 0.51 \text{ cm}^3 \text{ cm}^{-3}$. Such an estimate is in good agreement with the wet soils in the Kansas prairie (see Table 2). Extrapolation to $\Lambda = 0.0$ reveals that $\theta = 0.05 \text{ cm}^3 \text{ cm}^{-3}$ which is the average residual moisture content.

Normalizing soil moisture by rearranging the data in Fig. 2 between 0 (oven dry) and 1 (full saturation) allows the empirical function to be applied to a wider range of soil types as it excludes soil specific limits such as saturated soil water content and dry bulk density. The following relationship is then derived:

$$\Lambda = \lambda E / (\lambda E + H) = a + b \ln(\theta/\theta_{\text{sat}}) \quad (2)$$

or

$$\theta/\theta_{\text{sat}} = \exp\{(\Lambda - a)/b\} \quad (3)$$

where a and b = curve-fitting parameters; $a = 1.0$ (for normalized soil moisture); and $b = 0.421$. The accuracy of this relationship has been validated further with data collected from irrigated plains in Pakistan and Mexico.

Soil Moisture Validation in Pakistan and Mexico

Pakistan

The validation of Eq. (3) is carried out in the Rechna Doab area of the Indus Basin irrigation system. The Rechna Doab is the interfluvial area between the Chenab and Ravi Rivers and contains mainly alluvial soils. It is one of the oldest and most intensively developed irrigated areas of Punjab, Pakistan. The major crops are rice, cotton, sugarcane and forage crops dominating in the summer season (*kharif*), and wheat and forage in winter (*rabi*). Two sites—Pindi Bhattian and Faisalabad—have been selected for conducting field measurements on surface energy balance partitioning and soil moisture.

The Pindi Bhattian experimental site is at the Soil Salinity Research Institute, which is located on the north–western border of Rechna Doab ($73^\circ 20' 50.2'' \text{ E}$, $31^\circ 52' 34.2'' \text{ N}$). The site is flat and situated at an altitude of 212 m above sea level. The average precipitation is approximately 500 mm year^{-1} . The fields have a rice-wheat rotation. The phreatic surface is approximately 2 m deep from the soil surface.

The second site is the experimental field of the Cotton Research Institute of Ayub Agricultural Research Institute, Faisalabad, which is situated in the center of the Rechna Doab ($73^\circ 2' 49.8'' \text{ E}$, $31^\circ 23' 26.2'' \text{ N}$). The flat area lies at an altitude of 130 m above sea level. The climate is drier than in Pindi Bhattian with an average annual precipitation of 360 mm. Cotton–wheat rotations are practiced in this area and the phreatic surface is fairly deep, approximately 10 m below the surface.

Bowen ratio towers were installed and operated from June 21 2000 to March 21 2001, at both experimental plots to measure directly the evaporative fraction Λ . Near-surface atmospheric profiles of temperature, humidity and wind speed were measured. In this method, the unitless Bowen ratio β is determined from the difference in vapor pressure d_e and temperature dT between the two observed levels

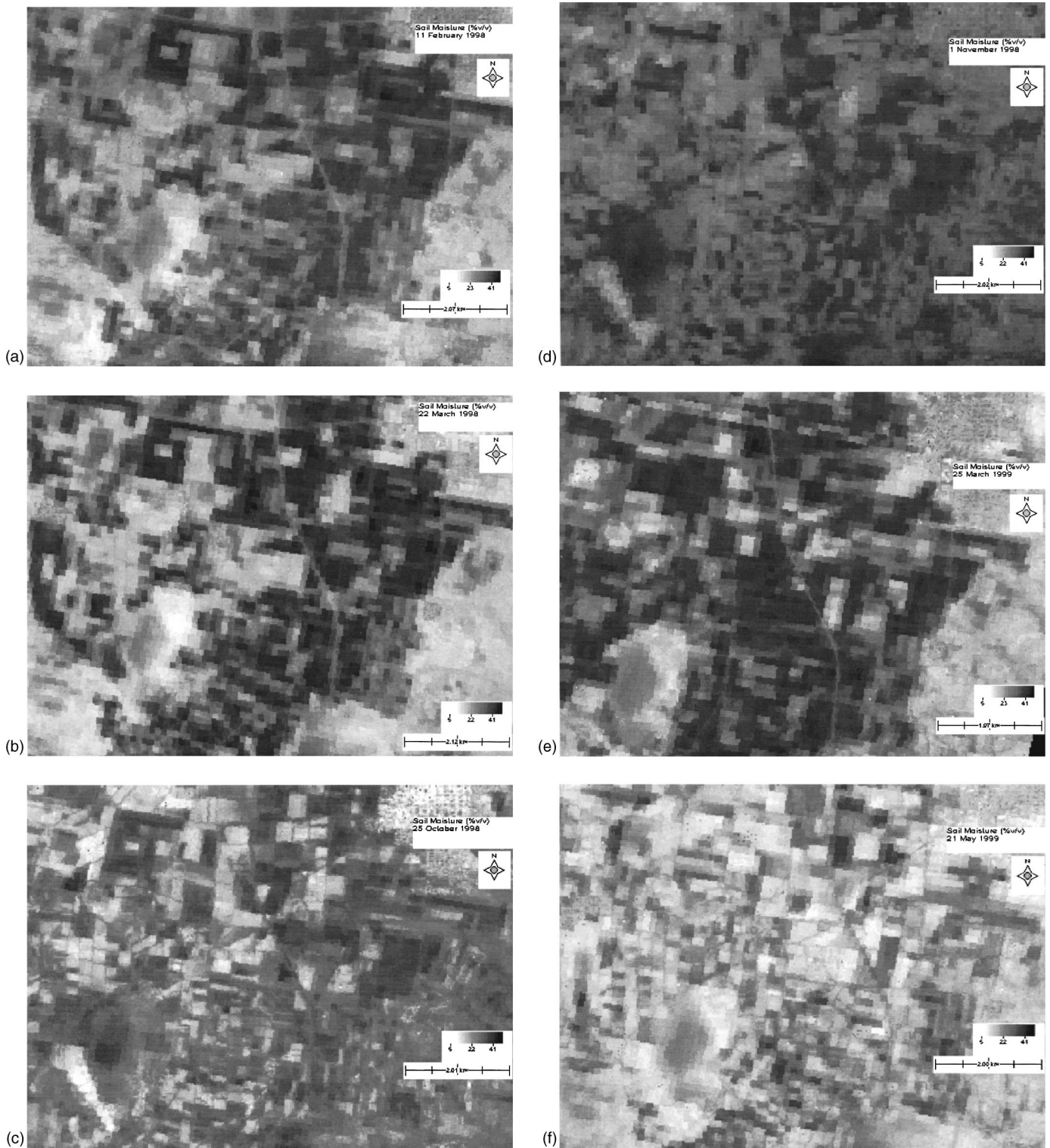


Fig. 6. Soil moisture, (a) 11 February 98; (b) 22 March 98; (c) 25 October 98; (d) 1 November 98; (e) 25 March 99; and (f) 21 May 99

$$\beta = \frac{H}{\lambda E} = \gamma \frac{T_{a_1} - T_{a_2}}{e_1 - e_2} \quad (4)$$

where γ (hPa K^{-1})=psychrometric constant; T_a (K)=air temperature; and e (hPa)=vapor pressure, subscripts 1 and 2 indicate the lower and upper levels, respectively. From β , the evaporative fraction Λ can be computed as

$$\Lambda = \frac{\lambda E}{\lambda E + H} = \frac{1}{1 + \beta} \quad (5)$$

The in situ meteorological measurements of evaporative fraction Λ have been used to estimate soil moisture content on the basis of the standard curve provided in Eq. (3). Saturated soil moisture contents θ_{sat} of 0.35 and 0.41 $\text{cm}^3 \text{cm}^{-3}$ for Faisalabad

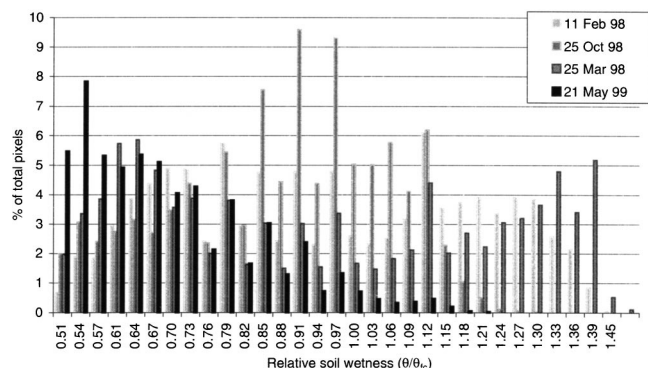


Fig. 7. Frequency distribution of relative soil wetness of irrigated plots in the 7,300 ha Cortazar, Mexico pilot area

and Pindi Bhattian, respectively, were used for this purpose. Soil moisture content in the root zone (up to 100 cm) was monitored in the field with the help of a theta probe based on the frequency domain technique. The theta probe measures the volumetric soil moisture content by measuring changes in the dielectric constant. The probes were installed at depth increments of 25 cm. The average of the four layers has been computed to obtain a value for the upper 100 cm. Measurements of the root depth in cotton and wheat revealed that most of the active roots are found in the first 100 cm and that only a very small fraction is deeper.

Mexico

The soils in the Lerma-Chapala basin in Mexico are vertisols with good water holding capacity. The average precipitation at Cortazar is approximately 650 mm year⁻¹; irrigation is from canals and wells. The topography is flat at an elevation of 1,700 m above mean sea level. Soil moisture at 45 cm depth was measured in fields near Cortazar (100° 59' 53.8" W, 20° 27' 26.3" N) using a capacitance probe calibrated for site soils based on previous gravimetric soil moisture measurements. Due to frequent deep irrigation applications, moisture did not vary considerably with depth. It is assumed that the depth of 45 cm represents the average value of soil moisture in the root zone. Soil moisture data were mainly collected from irrigated plots of wheat, alfalfa, and to a limited extent, strawberries. Except for strawberries, the majority of active roots are found in the first 100 cm below the surface. A soil water potential of -300 cm (pF 2.3) coincides with volumetric soil moisture content of approximately 0.35 cm³ cm⁻³. Moisture values between 0.30 and 0.45 cm³ cm⁻³ occur frequently. The maximum soil moisture content of 0.54 cm³ cm⁻³ was measured on 25 May 1999, and consequently a soil porosity of $\theta_{\text{sat}} = 0.54 \text{ cm}^3 \text{ cm}^{-3}$ has been considered in the fur-

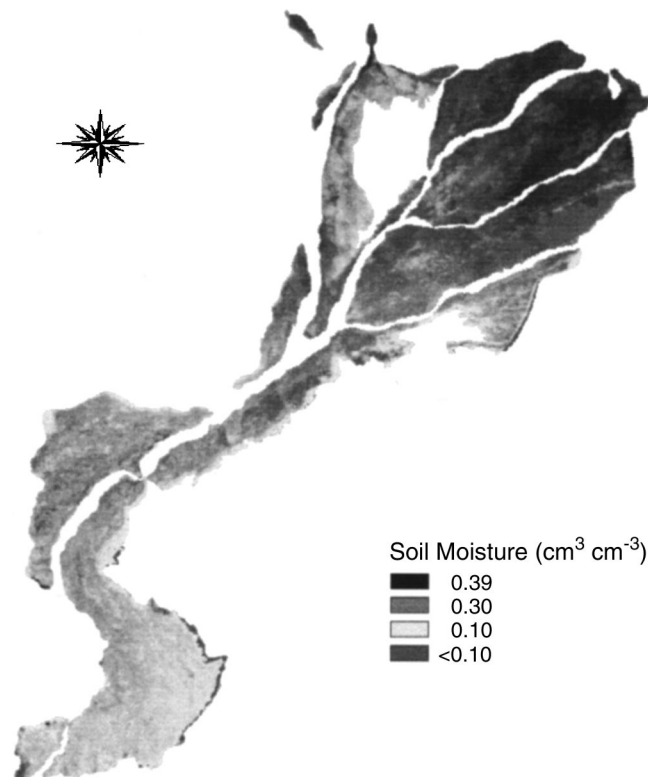


Fig. 8. Soil moisture content averaged over *rabi* (winter) season based on standard evaporative fraction–soil moisture curve [Eq. (3)] for entire 16 million ha Indus Basin, Pakistan

ther analysis of the Mexico data set. Although soil moisture measurements were collected throughout the 1998–1999 winter season, only data collected on 23 March 1999 could be used as they were close to the 25 May 1999 overpass date of a TM image used to compute the evaporative fraction with the SEBAL model.

Comparisons between evaporative fractions derived from high resolution TM images and evaporative fraction measurements on the ground have been made before in China (Wang et al. 1995) and Spain (Pelgrum and Bastiaanssen 1996) among other places. The agreement for desert surfaces, irrigated land, and dryland agriculture was good with differences between in situ measured and SEBAL-derived evaporative fractions on the order of 10–15% on a daily scale, which is also the uncertainty of the advanced eddy-covariance system itself. We therefore believe that the evaporative fraction for Cortazar computed from SEBAL has sufficient confidence to derive soil moisture maps. Fig. 3 compares measured values of soil moisture for the layer between 0 and 100 cm with soil moisture indirectly derived from the evapo-

Table 4. Soil Moisture Status of Irrigated Crops for the 7,300 ha Cortazar, Mexico Pilot Area

Date	Mean θ/θ_{fc} (–) all fields	Mean θ/θ_{fc} (–) irrigated fields	CV ^a (–) irrigated fields	Operational range (%) $0.8 < \theta/\theta_{fc} < 1.2$	Acceptable range (%) $0.6 < \theta/\theta_{fc} < 1.3$
11 Feb 98	0.65	0.95	0.29	46	56
22 Mar 98	0.93	0.95	0.31	32	76
25 Oct 98	0.85	0.88	0.27	68	93
21 May 99	0.58	0.69	0.30	21	70

Note: Percentage describes the fraction of pixels falling within the defined range.

^aCV is the coefficient of variation (standard deviation/mean).

rative fraction in Pakistan and Mexico. In Pakistan the evaporative fraction was measured in the field, while for Mexico it has been derived from a Landsat thematic mapper image. The root mean square (RMS) error is $0.049 \text{ cm}^3 \text{ cm}^{-3}$ if the standard curve presented in Eq. (3) is used and the average measured soil moisture content is $0.312 \text{ cm}^3 \text{ cm}^{-3}$. Hence the overall deviation is $0.049/0.312 \times 100\% = 15\%$.

A comparison of the soil moisture field measurements with the soil moisture determined from the standard curve reveals that there are no systematic errors present. The performance of Eq. (3) is equally good in moderately dry ($\theta \sim 0.15\text{--}0.20 \text{ cm}^3 \text{ cm}^{-3}$) and wet soils ($\theta \sim 0.40\text{--}0.45 \text{ cm}^3 \text{ cm}^{-3}$). The Pindi Bhattian rice fields seem to have the large deviations, but deviations on both sides of the 1:1 line are found, which implies that there is no bias present. Considering that Eq. (3) is based on prairies, vineyards, barley, and rainfed wheat and validated against irrigated wheat, alfalfa, cotton and rice, it is concluded that the effects from vegetation are minimal and that evaporative fraction is a reflection of the true status of the actual root zone soil water content. Further, the range of soil types does not seem to affect the accuracy. The scatter in Fig. 3 can be the result of the combined effect of a number of factors including instrument error in measuring soil moisture content, errors in Bowen ratio measurements, errors in the SEBAL parameterization of evaporative fraction, vertical variability of soil moisture content, crop roots not uniformly present throughout the root zone of 100 cm, etc. The deviation is, therefore, not necessarily an error of the estimation method, and error should consequently be considered smaller than the deviations presented in Fig. 4, the deviation probability distribution.

Fig. 4 reveals that on average, i.e., 50% of the cases, the absolute soil moisture content is off by approximately $0.035 \text{ cm}^3 \text{ cm}^{-3}$ or less. In 90% of the cases, the deviation is less than $0.07 \text{ cm}^3 \text{ cm}^{-3}$. The RMS error of $0.049 \text{ cm}^3 \text{ cm}^{-3}$ corresponds to 70% probability. For this reason, it is recommended that soil moisture estimates from evaporative fraction are presented with a class interval of $0.05 \text{ cm}^3 \text{ cm}^{-3}$, rather than in increments of $0.01 \text{ cm}^3 \text{ cm}^{-3}$. Consequently, the accuracy for estimating soil moisture at field capacity of a sandy soil with $\theta_{fc} = 0.15 \text{ cm}^3 \text{ cm}^{-3}$ is dissimilar to a clayey soil with $\theta_{fc} = 0.30 \text{ cm}^3 \text{ cm}^{-3}$. Hence, direct applications of the soil moisture detection technique presented here are less straightforward on eolic soils than on alluvial soils.

Applications

Irrigation Practices in Mexico

Several factors affect crop growth including soil structure, nutrient status, salinity, and farm practices. However, in low (or zero) rainfall conditions, moisture deficit exerts the most significant limitation on crop growth with the resulting dependence on irrigation. Water is delivered either through surface water canals or from groundwater. Canal irrigation requires appropriate coordination among the irrigation agency, often a water users association (or other intermediate body), and farmer water users. Because moisture adequacy is linked to the reliability of supply, which may be limited in large, relatively inflexible canal irrigation systems, farmers tend to apply water—sometimes in excess of soil water holding capacity or crop water demand—when it is available. Irrigation scheduling based on soil moisture status, not simply total irrigation application, is an important determinant of crop yields.

Thematic mapper imagery was acquired for portions of the basin during consecutive crop seasons in 1998 and 1999 (see Table 3). The particular area of study, located to the west of Cortazar town (Guanajuato state) in the Alto Rio Lerma Irrigation District, lies in the overlap of pass/row numbers 27/46, 28/45, and 28/46, permitting analysis of soil moisture for six dates over a 15-month period (see Fig. 5). Rainfall in Cortazar is unimodally distributed with 88% occurring in the June–September period. The primary cropping pattern is wheat/barley (December–May), maize/sorghum (June–October), with perennial alfalfa and a mix of horticultural crops.

The six resulting soil moisture images (Fig. 6) clearly show spatial and temporal trends in irrigation application and rainfall. The 1997 rainy season in the region was approximately 11% below average, resulting in low reservoir storage levels and the restriction of canal irrigation. As a result, soil moisture for February and March 1998 [Figs. 6(a and b)] was a result of groundwater irrigation, with saturated areas showing up in isolated patches around wells. Figs. 6(c and d) show the wider distribution of (lower value) moisture resulting from the 1998 rains. It is apparent from the differences in moisture that it rained between the 25 October 98 [Fig. 6(c)] and 1 November 98 [Fig. 6(d)]. It should be noted that irrigation only resumed for the planting of wheat in December where residual moisture was insufficient. The 25 March 99 image [Fig. 6(e)] shows the combined effect of groundwater and canal irrigation and should be contrasted with the 22 March 98 image [Fig. 6(b)], which shows only groundwater irrigation. Finally, the 21 May 99 image [Fig. 6(f)] was taken after the wheat harvest (with the last irrigation applied in early to mid April). High moisture areas on this image correspond to crops still under irrigation, particularly alfalfa.

A soil wetness performance indicator can be defined as the moisture content relative to field capacity, θ_{act}/θ_{fc} , to evaluate whether targets in irrigation supply are met. Bastiaanssen et al. (2001) termed this “relative soil wetness” with target values in an operational range between 0.8 and 1.2. The soil moisture content at field capacity for Cortazar was $\theta_{fc} \sim 0.35 \text{ cm}^3 \text{ cm}^{-3}$. The sub-area investigated with the 6 TM images specified in Table 3 occupies an area of approximately 7,300 ha. Irrigated land was discerned applying a threshold value of $\theta_{act}/\theta_{fc} \geq 0.5$, i.e., as $\theta_{act} \geq 0.18 \text{ cm}^3 \text{ cm}^{-3}$, assuming that drier soils are not irrigated. The frequency distribution and summary for four out of the six images are presented in Fig. 7 and Table 4. If we leave out the 21 May 1999 image, because only alfalfa was irrigated, the average percentage of irrigated pixels falling within the operational range becomes 49%. Due to weather parameters, the relative soil wetness in October lies more often in the operational range than for February and March. It is more difficult to keep the soil moisture in the operational range during February and March, and although the mean value of $\theta/\theta_{fc} = 0.95$ is high, February exhibits also a significant class of moisture values that are at the lower side. As the mean value is high, there must also be a large class of moisture values near full saturation. This agrees with earlier studies showing that the relative water supply in the Lerma-Chapala basin (Kloezen 1999; Scott et al. 1999) is high, and that groundwater users consume at least as much or more water than canal water users. Basically, the upper tail ends of the frequency distribution (see Fig. 8) reveal the groundwater irrigated plots where large amounts of water are dumped on the fields as the resource is not limited. The distribution of March 1998 shows an even greater bias towards full soil saturation, reflecting heavy overirrigation. Farmers can save significant pumping costs by extracting less groundwater and target irrigation more in the operational

range of relative soil wetness. The May 1999 image shows that the study area has dried down to $\theta/\theta_{fc}=0.58$, which is far below field capacity. This is when the crops have been harvested.

Water Resources Distribution Across Indus Basin, Pakistan

The second example in this paper comes from Pakistan, where upstream and downstream users in the Indus River system often have conflicts over water resources distribution. The average soil moisture content was computed from 12 individually acquired images during November 1993–April 1994. Fig. 8 demonstrates that the downstream riparians indeed have a lower soil moisture status than upstream agricultural users. These results are based on the application of low spatial resolution National Oceanographic and Atmospheric Agency—Advanced Very High Resolution Radiometer (NOAA-AVHRR) images, which are freely downloadable and have a spatial resolution of 1 km. The AVHRR sensor covers an area 2,800 km wide; with one image, a basin as large as the Indus (16 million ha of irrigation) can be surveyed. Although this is outside the scope of mapping detailed soil moisture patterns, it shows the power of optical images to investigate the availability of water resources across huge river basins.

Conclusions

Determination of soil moisture is required for the quantification of a range of hydrological processes and ultimately for water resources decision making. Field-based methods are cumbersome, expensive, and provide data for limited spatial and temporal coverage. There is a need for rapid, less expensive and reliable techniques for soil moisture determination. This paper has briefly summarized the progress of soil moisture detection using remote sensing, and presents an alternative method to microwave techniques that is shown to be suitable for a range of crop and soil types. The soil water content derived from this method is associated with the depth where root water extraction is active. This depth has a dynamic behavior when crops emerge and are in vegetative development. The method has been calibrated for Spain and Kansas, and validated against data collected in Mexico and Pakistan. A standard relationship between heat flux partition—expressed as evaporative fraction—and soil moisture content in the root zone has been tested. The average error is $0.035 \text{ cm}^3 \text{ cm}^{-3}$ and 90% of the cases ($n=52$) have an error less than $0.07 \text{ cm}^3 \text{ cm}^{-3}$. The RMS error is $0.05 \text{ cm}^3 \text{ cm}^{-3}$ such that moisture class intervals of $0.05 \text{ cm}^3 \text{ cm}^{-3}$ can be mapped accurately.

High resolution thermal-infrared data, such as operationally collected by Landsat TM and ASTER, permit the calculation of a surface energy balance including the evaporative fraction. Based on the method presented here, the spatial and temporal distribution of soil moisture conditions can be determined for any watershed or basin without ground data requirements. An example was demonstrated for a 7,300 ha pilot area near Cortazar in the Alto Rio Lerma Irrigation District in Mexico, which reveals that groundwater irrigation holds the soil between field capacity and full saturation. 49% of the plots in the 7,300 ha Cortazar pilot area lie in the operational range of relative soil wetness for various seasons of the year, with significant overirrigation apparent. Groundwater users should target irrigation applications more in the operational range of relative soil wetness.

A single processed enhanced TM image costs US\$600, while image processing and interpretation of soil moisture cost approxi-

mately an additional US\$2,000 depending on the level of expertise and local wages. This translates into costs as low as US\$0.59 per thousand hectares on a single image, or US\$2.36 per thousand hectares for an agricultural season (four images). This method can equally be applied to high resolution ASTER images as well as NOAA-AVHRR and MODIS images that can be obtained from the world wide web. The latter category of low resolution images is more suitable for river basin planning purposes as demonstrated in the example from the Indus Basin in Pakistan.

Notation

The following symbols are used in this paper:

- a = curve-fitting parameter;
- b = curve-fitting parameter;
- e = vapor pressure;
- G = soil heat flux;
- H = sensible heat flux to air;
- R_n = net radiation at surface;
- T = air temperature;
- α = parameter from Priestley–Taylor evaporation formulation;
- β = Bowen ratio;
- γ = psychrometric constant;
- θ = soil moisture;
- θ_{sat} = saturated soil moisture;
- Λ = evaporative fraction; and
- λE = latent heat flux.

References

- Allen, R. G. (2000). "Using the FAO-56 dual crop coefficient method over an irrigated region as part of an evapotranspiration intercomparison study." *J. Hydrol.*, 229(1), 27–41.
- Allen, R. G., Morse, A., Tasumi, M., Bastiaanssen, W. G. M., Kramber, W., and Anderson, H. (2001). "Evapotranspiration from Landsat (SEBAL) for water rights management and compliance with multi-state water compacts." *Proc., IGARSS 2001*, Australia.
- Allen, R. G., Pereira, L. S., Raes, D., and Smith, M. (1998). "Crop evapotranspiration: Guidelines for computing crop water requirements." *Irrigation and Drainage Paper No. 56*, Food and Agriculture Organization, Rome.
- Arnold, J. G., Allen, P. M., and Bernhardt, G. (1993). "A comprehensive surface-groundwater flow model." *J. Hydrol.*, 142, 47–69.
- Bastiaanssen, W. G. M. (2000). "SEBAL based sensible and latent heat fluxes over the irrigated Gediz basin." *J. Hydrol.*, 229(1), 87–100.
- Bastiaanssen, W. G. M., Ahmad, M. D., and Chemin, Y. (2002). "Satellite surveillance of evaporative depletion across the Indus Basin." *Water Resour. Res.*, 38(12), 1273 (DOI: 10.1029).
- Bastiaanssen, W. G. M., and Bandara, K. M. P. S. (2001). "Evaporative depletion assessments for irrigated watersheds in Sri Lanka." *Irrig. Sci.*, 21, 1–15.
- Bastiaanssen, W. G. M., Brito, R. A. L., Bos, M. G., Souza, R. A., Cavalcanti, E. B., and Bakker, M. M. (2001). "Low cost satellite data for monthly irrigation performance monitoring: Benchmarks from Nilo Coelho, Brazil." *Irrig. Drain. Syst.*, 15, 53–79.
- Bastiaanssen, W. G. M., Menenti, M., Feddes, R. A., and Holtslag, A. A. M. (1998). "A remote sensing surface energy balance algorithm for land (SEBAL). 1. Formulation." *J. Hydrol.*, 212–213, 198–212.
- Bastiaanssen, W. G. M., Molden, D. J., and Makin, I. W. (2000). "Remote sensing for irrigated agriculture: Examples from research and possible applications." *Agric. Water Manage.*, 46, 137–155.
- Bastiaanssen, W. G. M., Pelgrum, H., Droogers, P., de Bruin, H. A. R., and Menenti, M. (1997). "Area-average estimates of evaporation,

- wetness indicators and top soil moisture during two golden days in EFEDA." *Agric. Meteorol.*, 87, 119–137.
- Belmans, C., Wesseling, J. G., and Feddes, R. A. (1983). "Simulation of the water balance of a cropped soil: SWATRE." *J. Hydrol.*, 63, 271–286.
- Bolle, H. J., et al. (1993). "EFEDA: European field experiments in a desertification-threatened area." *Ann. Geophys.*, 11, 173–189.
- Davies, J. A., and Allen, C. D. (1973). "Equilibrium, potential and actual evapotranspiration from cropped surfaces in southern Ontario." *J. Appl. Meteorol.*, 12, 649–657.
- de Bruin, H. A. R. (1983). "A model for the Priestley–Taylor parameter alpha." *J. Clim. Appl. Meteorol.*, 22, 572–578.
- Droogers, P., Abeele, v. d., G. D., Cobbaert, J., Kim, C. P., Rosslerova, R., Soet, M., and Stricker, J. N. M. (1993). "Basic data sets description and preliminary results of EFEDA-Spain." *Rep. No. 37*, Wageningen Agricultural Univ., Wageningen, The Netherlands.
- Engman, E. T., and Chauhan, N. (1995). "Status of microwave soil moisture measurements with remote sensing." *Remote Sens. Environ.*, 51, 189–198.
- Hoeben, R., and Troch, P. A. (2000). "Assimilation of active microwave observation data for soil moisture profile estimation." *Water Resour. Res.*, 36(10), 2805–2819.
- Jackson, T. J. (1997). "Soil moisture estimation using spectral satellite microwave/imager satellite data over a grassland region." *Water Resour. Res.*, 33(6), 1475–1484.
- Jackson, R. D., Idso, S. B., Reginato, R. J., and Pinter, P. J. (1981). "Canopy temperature as a crop water stress indicator." *Water Resour. Res.*, 17, 1133–1138.
- Jackson, R. D., Reginato, R. J., and Idso, S. B. (1977). "Wheat canopy temperature: A practical tool for evaluating water requirements." *Water Resour. Res.*, 13, 651–656.
- Kloezen, W. H. (1999). "Measuring land and water productivity in a Mexican irrigation district." *Int. J. Water Resour. Dev.* 14(2), 231–247.
- Kustas, W. P., Zhan, X., and Jackson, T. J. (1999). "Mapping surface energy flux partitioning at large scales with optical and microwave remote sensing data from Washita '92." *Water Resour. Res.*, 35(1), 265–277.
- Li, J., and Islam, S. (1999). "On the estimation of soil moisture profile and surface fluxes partitioning from sequential assimilation of surface layer soil moisture." *J. Hydrol.*, 220(1/2), 86–103.
- Mahfouf, J. F. (1991). "Analysis of soil moisture from near-surface parameters: A feasibility study." *J. Appl. Meteorol.*, 30, 1534–1548.
- Mancini, M., Hoeben, R., and Troch, P. (1999). "Multifrequency radar observations of bare surface soil moisture content: A laboratory experiment." *Water Resour. Res.*, 35(6), 1827–1838.
- Molden, D., Sakthivadivel, R., and Keller, J. (2001). "Hydronomic zones for developing basin water conservation strategies." *Research Rep. No. 56*, International Water Management Institute, Colombo, Sri Lanka (www.iwmi.org)
- Monteny, B. A., et al. (1997). "The role of the Sahelian biosphere on the water and the CO₂ cycle during the HAPEX-Sahel experiment." *J. Hydrol.*, 188–189, 516–535.
- Moran, M. S., Clarke, T. R., Inoue, Y., and Vidal, A. (1994). "Estimating crop water deficit using the relation between surface-air temperature and spectral vegetation index." *Remote Sens. Environ.*, 49(2), 246–263.
- Moran, M. S., Hymer, D. C., Qi, J., and Kerr, Y. (2002). "Comparison of ERS-2 SAR and Landsat TM imagery for monitoring agricultural crop and soil conditions." *Remote Sens. Environ.*, 79, 243–252.
- Morse, A., Tasumi, M., Allen, R. G., and Kramber, W. J. (2000). "Application of the SEBAL methodology for estimating consumptive use of water and streamflow depletion in the Bear River Basin of Idaho through remote sensing." *Idaho Department of Water Resources Rep.*, Univ. of Idaho, Id.
- Njoku, E. G., and Entekhabi, D. (1996). "Passive microwave remote sensing to soil moisture." *J. Hydrol.*, 184, 101–129.
- Oki, T., Nishimura, T., and Dirmeyer, P. (1999). "Assessment of land surface models by runoff in major river basins of the globe using Total Runoff Integrating Pathways (TRIP)." *J. Meteorol. Soc. Jpn.*, 77, 235–255.
- Owe, M., and van de Griend, A. A. (1990). "Daily surface moisture model for large area semi-arid land applications with limited climate data." *J. Hydrol.*, 121, 119–132.
- Pelgrum, H., and Bastiaanssen, W. G. M. (1996). "An intercomparison of techniques to determine the area-averaged latent heat flux from individual in situ observations: A remote sensing approach using EFEDA data." *Water Resour. Res.*, 32(9), 2775–2786.
- Refsgaard, J. C. (1997). "Parameterization, calibration and validation of distributed hydrological models." *J. Hydrol.*, 198, 69–97.
- Sarwar, A., Bastiaanssen, W. G. M., Boers, T. M., and van Dam, J. C. (2000). "Evaluating drainage design parameters for the Fourth Drainage Project, Pakistan by using SWAP model. 1: Calibration." *Irrig. Drain. Syst.*, 14, 315–324.
- Schmugge, T. J. (1999). "Applications of passive microwave observations of surface soil moisture." *J. Hydrol.*, 212–213, 188–197.
- Scott, C. A., Palacios, E., and Bolaños, M. (1999). "Remote sensing assessment of the extent of groundwater irrigation in the Lerma-Chapala Basin, Mexico." *Proc., Int. Symp. on Integrated Water Management Agriculture*, Gómez Palacio, Mexico.
- Sellers, P. J., Hall, F. G., Asrar, G., Strebel, D. E., and Murphy, R. E. (1992). "An overview of the First International Satellite Land Surface Climatology Project (ISLSCP) Field Experiment (FIFE)." *J. Geophys. Res.*, 97(D17), 18345–18371.
- Smith, E. A., et al. (1992). "Area-averaged surface fluxes and their time-space variability of the FIFE experimental domain." *J. Geophys. Res.*, 97(D17), 18599–18622.
- Su, Z., Troch, P. A., and de Troch, F. P. (1997). "Remote sensing of bare surface soil moisture using EMAC/ESAR data." *Int. J. Remote Sens.*, 18(10), 2105–2124.
- Ulaby, F. T., and Elachi, C., eds. (1990). *Radar polarimetry for geoscience applications*, Artech House, London.
- van Oevelen, P. J. (1998). "Soil moisture variability: A comparison between detailed field measurements and remote sensing measurement techniques." *Hydro. Sci. J.*, 43(4), 511–520.
- Verhoest, N. E. C., Troch, P. A., Paniconi, C., and de Troch, F. P. (1998). "Mapping basin scale variable source areas from multitemporal remotely sensed observations of soil moisture behavior." *Water Resour. Res.*, 34(12), 3235–3244.
- Wagenet, R. J., and Hutson, J. L. (1996). "Scale-dependency of solute transport modeling/GIS applications." *J. Environ. Qual.*, 25(3), 499–510.
- Walker, J. P., and Houser, P. (2001). "A methodology for initializing soil moisture in a global climate model: Assimilation of near-surface soil moisture observations." *J. Geophys. Res.*, 106(D11), 11761–11774.
- Wang, J., Ma, Y., Menenti, M., Bastiaanssen, W. G. M., and Mitsuta, Y. (1995). "The scaling up of processes in the heterogeneous landscape of HEIFE with the aid of satellite remote sensing." *J. Meteorol. Soc. Jpn.*, 73(6), 1235–1244.